Experimental Study of the Influence of the Flow Rates in SMB Chromatography

Tong Yun, Guoming Zhong and Georges Guiochon
Dept. of Chemistry, University of Tennessee, Knoxville, TN 37996
Div. of Chemical and Analytical Services, Oak Ridge National Laboratory, Oak Ridge, TN 37831

A Sorbex-type SMB separation instrument was operated for the separation of mixtures of 2-phenyl ethanol and 3-phenyl-1-propanol on a series of eight columns packed with Zorbax C18 bonded silica, using a 60:40 (v/v) solution of methanol and water as the mobile phase. The experiments were carried out with low-concentration mixtures under linear conditions. The elution profiles of both compounds between any two successive columns of the set under steady-state conditions were recorded while compositions of the raffinate and extract were measured. The four safety margin factors, β_j, were divided into two groups: β_1 and β_4; β_2 and β_3 with different influence. Within the framework of the linear, ideal model of chromatography, a range of flow rates enables an SMB to operate successfully by completely separating the feed into its two components. The influence of different flow rates on the performance of the separator was studied by calculations and experiments with excellent agreement between both sets. With a simple optimization strategy, the four flow rates are selected to maximize the production rate or the concentration of extract and raffinate products, or to minimize the desorbent consumption. These optimum conditions are obtained by controlling the locations of concentration profiles inside the SMB. A reliable model for SMB operation allows a rapid and easy selection of the optimum experimental conditions.

Introduction

Simulated moving-bed separations (SMB) have been attracting considerable attention since it became obvious that this method is ideally suited to the purification of enantiomers required by the pharmaceutical industry and, more recently, the agrochemical industry for many intermediates and/or final products (Stinson, 1995). Although the process is now more than 35 years old (Broughton and Gerhold, 1961), most of its industrial applications have so far been carried out in the linear range of the equilibrium isotherm. Pioneering works by Ruthven and Ching (1989) and, more recently, by Fish et al. (1993) and by Storti et al. (1993) have secured a basic understanding of the process. In spite of this fundamental knowledge, a number of issues of practical importance remain without simple solutions.

Paramount among these issues are the determination of optimum design and operation conditions. They involve the optimum characteristics of the column and their arrangement (i.e., ideal number of columns per section). Among the most critical is selecting the optimum flow rates of the four liquid streams and the solid phase. Presently, these optimizations are carried out on an empirical basis. Because of the inertia of the SMB units which reach steady-state operation after a rather large number of cycles and of the risk of "crashing" the unit, empirical adjustments are long, tedious and expensive due to production lost and solvent wasted. Simple theoretical considerations, if supported by adequate experimental results, could become most useful and save considerable effort and means by allowing start-up to be carried out under nearly optimal conditions.

The recent development of an algebraic solution of the ideal model of SMB under linear conditions (Zhong and Guiochon, 1996) offer such a simple and practical approach. Initially developed for a four-column SMB, with one column per section, this solution can be extended to the case of any number of columns in each section (see Appendix A). It gives the concentration profiles of the raffinate and the extract

Correspondence concerning this article should be addressed to G. Guiochon.

along the four sections of a Sorbex SMB and the concentration histories at the extract and the raffinate ports. Because it is algebraic and a function of the cycle rank, the solution for the limit number of an infinity of cycles can readily be calculated. Hence, the algebraic solution under steady-state conditions is available. The effects of a finite rate of mass transfer or of an axial dispersion observed in real units, which use columns with a finite efficiency, could be estimated from the known influence of apparent dispersion in chromatographic columns under linear conditions. The use of a linear model to investigate the properties of the SMB separator is relevant because the equilibrium isotherms of the two feed components are linear and noncompetitive in a number of industrial applications. The equilibrium isotherms of fructose and glucose on ion-exchange resins are linear in a wide concentration range (Ching and Ruthven, 1985; Howard et al., 1988). Isotherms are also linear and noncompetitive in size exclusion chromatography, a mode of chromatography which is widely used for the separation of high-molecular-weight compounds (Barker et al., 1983).

The algebraic solution previously published assumes that the values of β_j, the conventional safety factors of Ruthven and Ching (1989), which relate the mass flow rates of the two feed components in the liquid and the solid phases, are the same in all the sections of the unit. This simplifying assumption is not necessary. The algebraic solution of the ideal, linear model can be extended to the case of different values of β_j in each section (Zhong et al., 1997). It will be used here. This article shows how these new theoretical advances can be used to solve some problems of practical importance. First, we discuss the consequences of the choice of different flow-rate safety-margin factors on the performance of an SMB unit with two columns per section. Second, we demonstrate an excellent agreement between the predictions of simple arithmetic calculations and the experimental results obtained with a laboratory SMB unit.

Model of Simulated Moving Bed

The system studied in this work is an SMB of the Sorbex type (Broughton, 1985), as illustrated in Figure 1 of Zhong et al. (1997). The modeling consists of three parts: the column model, the node model, and the separation conditions (Zhong and Guiochon, 1996; Yun et al., 1997).

Column model

The columns used in the experiment have an efficiency of approximately 3,000 plates. Hence most of the dispersion undergone by the bands takes place in the pumps and the long tubing going from the valves to the raffinate and extract pumps and then to detectors (Yun et al., 1997). This kind of mixing, which takes place outside of the separation unit, has little effect on the overall separation of the feed components and cannot be detected by the on-line detector located in the main SMB stream, between the two columns, as illustrated in Figure 1b.

Two different column models were employed: the ideal model and the equilibrium-dispersive model (Guiochon et al., 1994). The mass balance equation in column j (j = I, II, III, IV) for component i (i = 1, 2) is written:

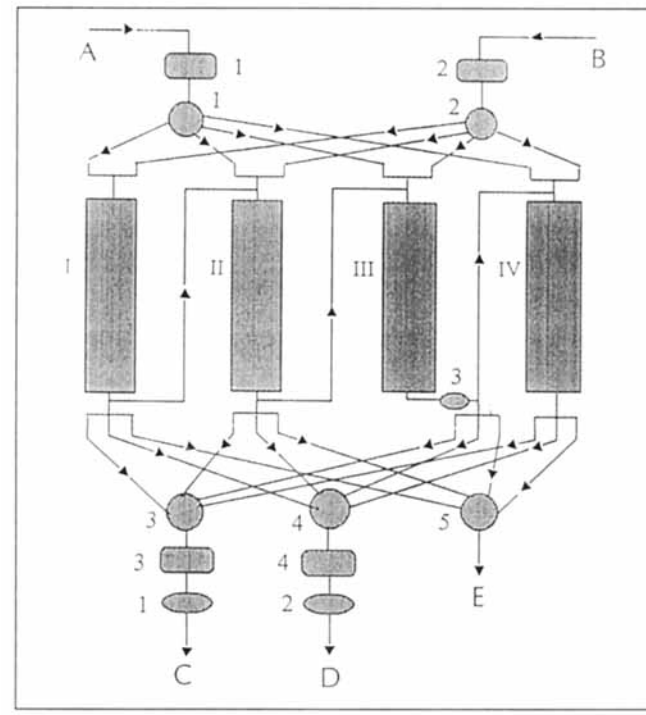

Figure 1. SMB experimental unit.

Connections to outside: A = feed; B = solvent; C = raffinate; D = extract; E = recycle. Pumps (rectangular boxes): 1 = feed; 2 = solvent, 3 = raffinate; 4 = extract. Rotary valves (circular boxes): 1 = feed; 2 = solvent; 3 = raffinate; 4 = extract; 5 = recycle. Detectors (oval boxes): 1 = raffinate; 2 = extract; 3 = on-line detector.

$$\frac{\partial C_{i,j}}{\partial t} + u_j \frac{\partial C_{i,j}}{\partial z} + F \frac{\partial q_{i,j}}{\partial t} = D_L \frac{\partial^2 C_{i,j}}{\partial^2 z} \tag{1}$$

where $C_{i,j}$ and $q_{i,j}$ are the liquid- and solid-phase concentrations of component i in column j, respectively; u_j is the velocity of the liquid phase in column j; D_L is the axial dispersion coefficient of the solutes (assumed to be the same for two closely related components); $F = (1 - \epsilon_T)/\epsilon_T$ is the phase ratio; ϵ_T is the column total porosity. $D_L = 0$ corresponds to the ideal model (columns of infinite efficiency).

A linear isotherm is considered:

$$q_{i,j} = K_i C_{i,j} \tag{2}$$

We assume that component 1 is less retained than component 2 at infinite dilution: $K_1 < K_2$. The separation factor is $\alpha = K_2/K_1 > 1$.

The initial and boundary conditions in the case of SMB operations are:

$$C_{i,j}(z,0) = 0, \qquad q_{i,j}(z,0) = 0 \tag{3a}$$

$$u_j C_{i,j}(0,t) - D_L \frac{\partial C_{i,j}}{\partial z}(0,t) = u_j C_{i,j}^{\text{in}} \tag{3b}$$

$$\frac{\partial C_{i,j}}{\partial z}(L,t) = 0 \tag{3c}$$

where $C_{i,j}^{in}$ is the concentration at each column inlet, which is supplied by the relevant node mass balance equation (see next section). Equation 3b is Danckwerts condition. This set of conditions is a general condition. However, when these conditions are applied to the ideal model, D_L is set equal to 0.

The solvent, feed, and draw-off nodes are shifted after a certain time or cycle time, t^*, to the next position along the liquid flow direction. This creates the simulated countercurrent movement of the solid phase required in SMB, as shown in Figure 1 of Zhong et al. (1997). At the beginning of a new cycle, the initial and boundary conditions of each column are updated according to the concentration profiles in different sections of the SMB at the end of the previous cycle.

An algebraic solution of the linear, ideal model is available for the concentration histories at the raffinate and extract ports and the concentration profiles of both components along the columns of an SMB in the case of one column per section (Zhong and Guiochon, 1996). This solution assumes that the value of β_j (Eqs. 6a–6d) is the same in all four sections. The solution in the case of eight columns (two per section) with different values of β_j in each section is described in Appendix A. Numerical solutions were calculated using a program implementing the equilibrium-dispersive model (Guiochon et al., 1994).

Node model

The flow and integral mass balance equations at each node are given by the following equations in which $Q_{\rm I}$, $Q_{\rm II}$, $Q_{\rm III}$, $Q_{\rm IV}$ are the flow rates through the corresponding columns, Q_D is the desorbent flow rate, Q_E, the extract flow rate, Q_F, the feed flow rate, and Q_R, the raffinate flow rate. These equations are integral mass balances, which assume that there is no dispersion at these nodes.

Desorbent Node (Eluent):

$$Q_{\rm IV} + Q_D = Q_{\rm I}$$

$$C_{i,{\rm IV}}^{\rm out} Q_{\rm IV} + C_{i,D} Q_D = C_{i,{\rm I}}^{\rm in} Q_{\rm I} \tag{4a}$$

Extract Drawoff Node:

$$Q_{\rm I} - Q_E = Q_{\rm II}$$

$$C_{i,{\rm I}}^{\rm out} = C_{i,{\rm II}}^{\rm in} = C_{i,E} \tag{4b}$$

Feed Node:

$$Q_{\rm II} + Q_F = Q_{\rm III}$$

$$C_{i,{\rm II}}^{\rm out} Q_{\rm II} + C_{i,F} Q_F = C_{i,{\rm III}}^{\rm in} Q_{\rm III} \tag{4c}$$

Raffinate Drawoff Node:

$$Q_{\rm III} - Q_R = Q_{\rm IV}$$

$$C_{i,{\rm III}}^{\rm out} = C_{i,{\rm IV}}^{\rm in} = C_{i,R} \tag{4d}$$

where $C_{i,j}^{\rm out}$ and $C_{i,j}^{\rm in}$ are the concentrations of component i at the outlet and the inlet of column j, respectively, and Q_j is the flow rate through column j, related to the liquid phase velocity by $Q_j = \epsilon_T A u_j$, where A is the column geometrical cross-sectional area.

Separation condition

Let us first define $\gamma_{i,j}$ as the net ratio between the mass flow rates of component i in the liquid and the solid phases in the section j. Ruthven and Ching (1989) have shown that $\gamma_{i,j}$ is the key parameter in the operating design of an SMB

$$\gamma_{i,j} = \frac{Q_s q_{i,j}}{Q_j C_{i,j}} = \frac{(1-\epsilon_T) u_s q_{i,j}}{\epsilon_T (u_j - u_s) C_{i,j}} \xrightarrow{\text{if linear isotherm}} \frac{F u_s K_i}{u_j - u_s} \tag{5}$$

where $Q_s = (1-\epsilon_T) A u_s$ is the solid phase flow rate and K_i is the slope of the isotherm. The mass flow rates in the liquid phase in Eq. 5 are corrected to account for the movement of the solid phase. For a true moving bed separator (TMB), $u_j - u_s$ would be replaced by u_j in the denominator of the terms of Eq. 5.

From the previous analysis of Ruthven and Ching (1989), the following conditions have to be fulfilled in order to reach a stable operation and to achieve separation between the two components of the feed in a TMB

$$\text{in Section I} \quad \gamma_{1,{\rm I}} < 1, \quad \gamma_{2,{\rm I}} < 1 \tag{6a}$$

$$\text{in Section II} \quad \gamma_{1,{\rm II}} < 1, \quad \gamma_{2,{\rm II}} > 1 \tag{6b}$$

$$\text{in Section III} \quad \gamma_{1,{\rm III}} < 1, \quad \gamma_{2,{\rm III}} > 1 \tag{6c}$$

$$\text{in Section IV} \quad \gamma_{1,{\rm IV}} > 1, \quad \gamma_{2,{\rm IV}} > 1 \tag{6d}$$

These eight relationships can be reduced to only four according to Ruthven and Ching (1989) because in sections I and III the more adsorbed component is the critical component while in sections II and IV it is the less adsorbed component which is the critical one. Zhong and Guiochon (1996) have used a single safety margin factor for all the sections, β, defined as the ratio of the net mass flow rates of the critical component of the feed in the liquid and the solid phases. The ratio is written so that β is larger than 1. They found that the SMB operation is stable and effective only if the flow rates are selected so that $1 \le \beta \le \sqrt{\alpha}$.

However, we may accept a slightly more complex model and consider that there are four different safety margins, β_j with $j = 1, 2, 3$, or 4, one factor for each of the four different sections instead of a single one for all the sections. The critical coefficients are given by the following set of equations, valid for SMB

$$Q_{\rm I}/Q_S = K_2 \beta_1 + 1/F \tag{7a}$$

$$(Q_{\rm I} - Q_E)/Q_S = K_1 \beta_2 + 1/F \tag{7b}$$

$$(Q_{\rm I} - Q_E + Q_F)/Q_S = K_2/\beta_3 + 1/F \tag{7c}$$

$$(Q_{\rm I} - Q_E + Q_F - Q_R)/Q_S = K_1/\beta_4 + 1/F \tag{7d}$$

This new set is also more useful for practical applications than the previous one, as will be shown later in this work. Figures 2a and 2b illustrate the domain of the β_j space which contains the values for which it is possible to operate the SMB and achieve the separation of the two feed components.

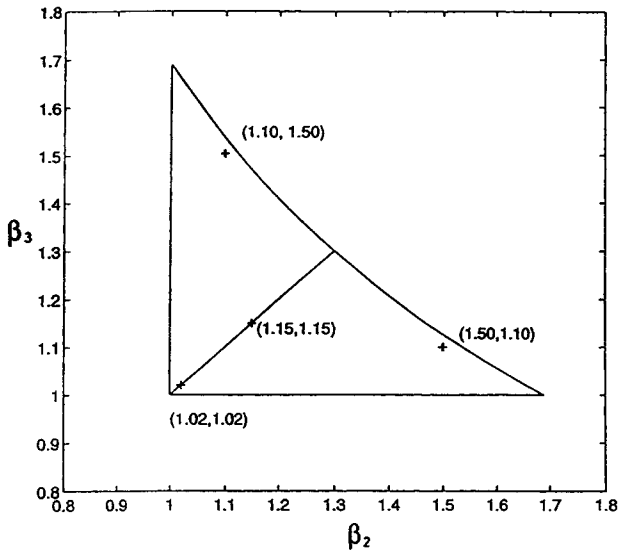

Figure 2a. Domain of possible values of β_2 and β_3 (α = 1.69).

All values inside the curvilinear, isosceles triangle are acceptable.

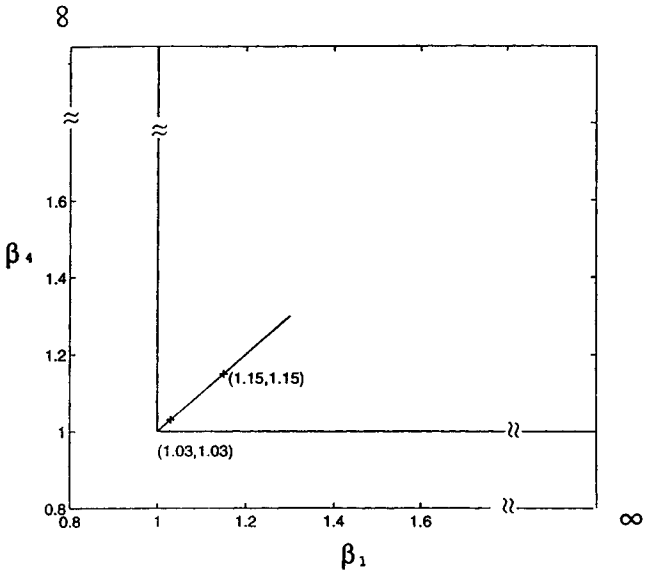

Figure 2b. Domain of possible values of β_1 and β_4 (α = 1.69).

All values larger than 1.0 are acceptable.

The four values, β_j, can be chosen independently, provided that they satisfy Eqs. B5a and B5b. To achieve the determination of the actual flow rates, we use the conventional relationship between the mass flow rate of the solid phase and the cycle time

$$Q_S = \frac{(1-\epsilon_T)LA}{t^*} \tag{8}$$

where L is the column length and A its geometrical cross-section area.

Note that, when an SMB unit has been designed and built, there are five operating parameters, the cycle time (i.e., the solid phase mass flow rate), and the four β_j values. Although there are four solution flow rates which can be adjusted, those of the desorbent, the feed, the raffinate, and the extract, there is an integral balance relationship between these flow rates, the sum of the desorbent and feed flow rates being equal to the sum of the raffinate and extract flow rates. So, there are only four independent operation parameters. We have omitted the temperature from the list above. Operation is most often carried out at ambient temperature, as in the present work, but this is not necessarily so and this parameter must be considered.

Experimental Setup

Exactly the same instrument was used for the acquisition of the data in our previous study (Yun, 1996; Yun et al., 1997). It is shown in Figure 1.

SMB chromatography

The laboratory-scale continuous chromatography system (model ICLC 16-10, Prochrom, Indianapolis, IN; Champigneulles, France) used consists of four HP1050 pumps (Hewlett-Packard, Palo Alto, CA) for the feed, eluent, raffinate, and extract. Five electropneumatic 16-port valves (VALCO, Houston), controlled by a computer to actuate the SMB, are connected to the feed, solvent, raffinate, extract, and recycle ports, respectively. The system can be operated at a maximum inlet pressure of 70 atm. It can run with any number of columns in each of the four sections provided that the total number of columns be 16 or less. All the experiments were made with 8 columns. The flow rate delivered by each pump and the movement of each valve is controlled by the CHROSOFT software (Prochrom, 1996). The accuracy and stability of the flow rates delivered by the pumps is better than 0.003 mL/min.

The system includes three UV spectrophotometric detectors, all operating at 265 nm. The first two detectors (both Spectroflow 757, Applied Biosystems, Ramsey, NJ) were located on the extract and the raffinate lines, respectively, between the pump and the collector. They monitor the concentration histories at these two ports. The third detector (HP1100, Hewlett Packard, Palo Alto, CA), equipped with a high-pressure flow cell, was placed in the main solvent stream of the SMB between the end of a column section and a rotary valve. The signal recorded with this detector is related to the concentrations of the two components eluting from the column. Provided that the detector response is linear, its response equals $S_1C_1 + S_2C_2$, with S_i the response factor of component I. Knowing the concentration profiles of the two components along the series of columns in the SMB and the response factors allows the calculation of these elution profiles for any position of the detector in the SMB. Thus, this arrangement permits a comparison between the experimental and numerical results regarding these profiles. The concentrations used were low enough to achieve both linear isotherm behavior of the two components and a linear response of all three detectors (the stronger constraint of the two). The performance of the detectors was discussed by Yun et al. (1997).

Table 1. Characteristics of the Columns Used

Column No.	t_0 (min)	F	K_1	K_2	α	N_1	N_2	N_2/N_1
A	2.190	0.7565	1.386	2.326	1.678	2,304	2,271	1.015
B	2.202	0.7468	1.401	2.388	1.704	2,856	2,820	1.013
C	2.194	0.7532	1.403	2.376	1.694	3,653	3,406	1.073
D	2.194	0.7532	1.405	2.362	1.687	1,742	1,756	0.992
E	2.189	0.7572	1.400	2.354	1.681	3,810	3,610	1.055
F	2.190	0.7565	1.424	2.405	1.689	2,006	2,049	0.979
G	2.201	0.7476	1.400	2.380	1.700	3,739	3,643	1.026
H	2.192	0.7549	1.351	2.283	1.690	4,261	4,181	1.019
Avg.	2.194	0.7532	1.397	2.359	1.690	3,046	2,967	1.021
RSD (%)	0.22	0.53	1.51	2.96	0.52	31	29.5	3

Flow rate = 2 mL/min; component 1 = 2-phenylpropanol; component 2 = 3-phenyl-1-propanol.

Columns and chemicals

The system was fitted with eight columns (1.0 cm × 9.8 cm) packed with 10-μm Zorbax spherical C-18 bonded silica (BTR, Wilmington, DE). Table 1 shows the parameters of the eight columns and their performance (Yun et al., 1997). The column-to-column fluctuations of the holdup time, phase ratio and retention factor have all a relative standard deviation (rsd) of 0.5% or lower. The column efficiency is much less reproducible than any of the other column parameters (rsd of about 30%). The eight columns are assembled in four sections of two columns each.

2-Phenyl ethanol and 3-phenyl-1-propanol were purchased from Fluka (Ronkonkoma, NY). 2-Phenyl ethanol ($K_1 = 1.397$) is less retained than 3-phenyl-1-propanol ($K_2 = 2.359$). The value of the separation factor, $\alpha = 1.69$, makes the separation of these two components rather easy to perform with an SMB.

The mobile phase was a 60:40 methanol/water (v/v) solution. All other concentrations are reported in mg/mL. A concentration of 1 mg/mL corresponds to molarities of 8.2 mM for 2-phenyl ethanol and 7.4 mM for 3-phenyl-propanol. Methanol and water were purchased from Burdick and Jackson (Muskegon, MI). All products were used without further purification.

Results and Discussion

Selection of the values for β_j

As explained in Appendix B, the set of β_j values can be divided into two groups, (β_2, β_3) and (β_1, β_4). Values of the first group (β_2, β_3) control the separation. Values of the second group (β_1, β_4) control the product recovery and the solvent consumption. The fact that the two groups can be treated separately is specific to the use of a linear isotherm. Obviously, it simplifies considerably the optimization of the experimental conditions.

Figure 2a illustrates the constraints for β_2 and β_3 (Eqs. B5a). The point of coordinates (β_2, β_3) must be inside the curvilinear triangle shown in the middle of the figure. The straight segment between the points of coordinates (1,1) and ($\sqrt{\alpha}$, $\sqrt{\alpha}$) represents the set of possible values of β under the simplified condition $\beta_j = \beta(\forall i)$ of the same safety margin for all sections. Figure 2b illustrates the constraints derived for β_1 and β_4 (Eqs. B5a). In this case, the condition is much less restrictive since it resumes to $\beta_1 > 1$ and $\beta_4 > 1$ and the entire quadrant is available. The straight segment between points (1,1) and ($\sqrt{\alpha}$, $\sqrt{\alpha}$) represents the condition obtained when the same safety margin is assumed for all the four sections.

The parameter β_1 can take any value larger than 1. A value of 1 corresponds to the minimum flow rate possible in section I (Eq. B5b). An infinite value of β_1 corresponds to an infinite liquid-phase flow rate in this section. Accordingly, with $\beta_1 = 1$, one will get the most concentrated extract possible while taking the risk that section I (used as section IV after the next column switching) may not be fully regenerated, the desorbent recycle becomes contaminated with extract, some extract is passed on to section IV, and hence a certain amount of component 2 ends up into the raffinate due to the flow rate in section IV lower than that in section I. Conversely, with $\beta_1 = \infty$, one will get a zero concentration of the extract produced but section I will certainly be fully cleaned of extract. A high value of β_1 ensures a high extract purity. Similarly, β_4 can take any value larger than 1. When $\beta_4 = 1$, Q_{IV} takes the maximum possible value (Eq. B5b), the concentration of the raffinate will be maximized with the lowest possible consumption of desorbent (Eq. B1d). Conversely, when $\beta_4 = \infty$, the concentration of the raffinate produced is the lowest possible, no flow of desorbent enters section IV (Eq. B5b, $Q_{IV} = 0$), which corresponds to the three-section SMB configuration in which there is no desorbent recovery function.

Results in Table 2 can help optimize the performance of an SMB under linear conditions, at least when the two components are completely separated. To maximize the feed flow rate and decrease the desorbent consumption, the four β_j values must be as small as possible. However, decreasing β_2 also increases Q_E and hence produces less concentrated extract. Decreasing β_3 increases Q_R and hence produces less concentrated raffinate. Depending on the exact optimum conditions of a given separation, different compromises will have to be adopted.

Experimental results vs. solutions of ideal and equilibrium-dispersive models

The Sorbex-type SMB used in this work has two columns in each section. Three different sets of experimental conditions were studied. The data points representing these different conditions are shown in Figures 2a and 2b. The concentration profiles are shown in Figures 3 to 5. Figures 3a, 4a and 5a compare the detector signal recorded by the on-line detector and the profiles derived from the theory of linear SMB. These figures are mosaics obtained by placing side by side the eight elution profiles recorded from a physical column located successively at each of the possible positions in

Table 2. Change of β_j Caused by an Increase in Each of the Four Flow Rates of an SMB Unit

	β_1	β_2	β_3	β_4
Q_F	na	↓	↓	na
Q_E	↑	↓	na	na
Q_R	na	na	↓	↑
Q_D	↑	na	na	↑

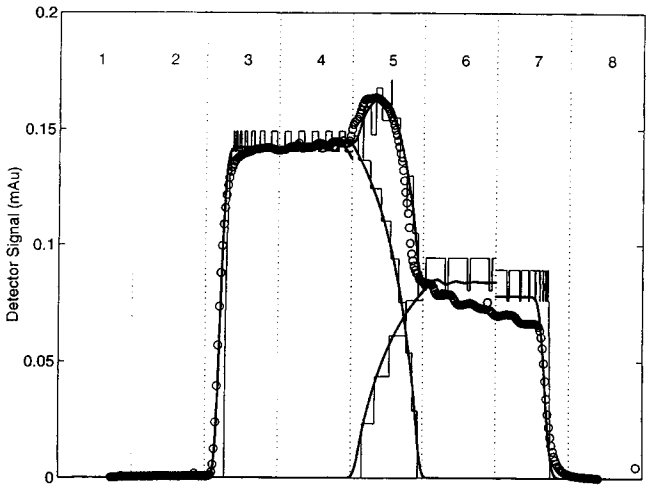

Figure 3a. Experimental results recorded with an on-line detector for $\beta_1 = \beta_2 = \beta_3 = \beta_4 = 1.15$

Total porosity of the column, $\epsilon_T = 0.572$. Flow rates: $Q_I = 1.436$ mL/min; $Q_{II} = 1.041$ mL/min; $Q_{III} = 1.201$ mL/min; $Q_{IV} = 0.902$ mL/min. Switching time, $t^* = 9.33$ min. Feed composition: $C_1 = 0.115$ g/L; $C_2 = 0.091$ g/L. Symbols, experimental data. Thick solid lines, concentration profiles of raffinate and extract calculated with the nonideal model. Thin solid line, concentration profiles of raffinate and extract calculated with the ideal model.

the schematics of the SMB (Figure 1). The solid lines in Figures 3a, 4a and 5a were derived from the concentration profiles calculated along the columns by eluting these profiles and multiplying the concentrations by the response factor of the detector (Yun et al., 1997). The calculated profiles were obtained either with the algebraic solution of the ideal model in Appendix A (thin solid line) or with the numerical solution of the equilibrium-dispersive model (thick solid line). Figures 3b, 4b and 5b show the axial concentration profiles at the end of a cycle (under steady-state conditions) calculated with the linear, ideal model (equations discussed earlier) and with the numerical solution of the equilibrium-dispersive model. Note that in Figures 3b, 4b, 5b, 6 and 7, the concentrations of the two components are normalized to the corresponding feed concentration. The extent of dilution of the feed due to the separation process is clear. In Figures 3a, 4a and 5a, the actual concentrations measured are reported. The switching times (t^*) used were nearly the same in all three cases. The value selected for the separation factor of the two components was $\alpha = 1.69$. The two components are completely separated under any of the three sets of operating conditions. The separation only takes place in columns II.2 and III.1 in the frame of the linear, ideal model and could have been carried out with a four-column SMB (Yun et al., 1997).

Under the first set of conditions (Figures 3a and 3b), the four β_j parameters have the same value, 1.15. The equations of the ideal model give the following values for the critical lengths of the problem (Appendix A): $L_d^0 = 0.206L$ (Eq. A3d), $n_e = 6$ (Eq. A4), $L_d^5 = 0.198L$ (Eq. A5), and $\Lambda_d^\infty = 1.543L$ (Eq. A7). So, the rear of component 2, which enters column II.2 at the beginning of the second cycle, appears in column II.1 for the first time at the beginning of the 6th cycle. Under steady-state conditions, the front shock of the band of component 2 is approximately halfway along column II.1. In section III of the SMB, $K_D = 0.2422$ (Eq. A2d) and $n_r = 5$ (Eq. A8), so the front of component 1 penetrates into section IV during the 5th cycle. The values of L_0^a (Eq. A3a), L_5^a (Eq. A11), and Λ_a^∞ (Eq. A13) are $0.242L$, $0.190L$, and $1.78L$, respectively. So, under steady-state conditions, the band front stays inside column IV.1 and does not reach column IV.2. There is no concentration of either component under steady-state conditions in panels 1, 2 and 8 of Figure 3a. This result is confirmed by the solution of the equilibrium-dispersive model (Figure 3b). Columns I.2 and IV.2 appear to be unnecessary to achieve the separation requested under this particular set of experimental conditions. The SMB would achieve the same performance without these two columns. Analyses of collected fractions of the SMB effluents were carried out as described previously (Yun et al., 1997). The extract contained 97.5% of 3-phenyl propanol and 2.5% of 2-phenyl ethanol, the raffinate, 99.5% of 2-phenyl ethanol and 0.5% of 3-phenyl propanol.

Under the second set of experimental conditions (Figures 4a and 4b), both β_2 and β_3 remain equal to 1.15, but we have chosen $\beta_1 = \beta_4 = 1.03$. This corresponds to the production of more concentrated extract and raffinate streams and to a lower solvent consumption. Since β_2 and β_3 remain unchanged, L_0^d and n_e are the same and only the values of L_d^5 and Λ_d^∞ are changed (section II). They become equal to $0.199L$ and $1.727L$, respectively. In section III, L_0^a and n_r are also unchanged, while L_5^a and Λ_a^∞ become equal to $0.164L$ and $1.96L$, respectively. Accordingly, although the ideal model profile does not enter into column IV.2, it gets very

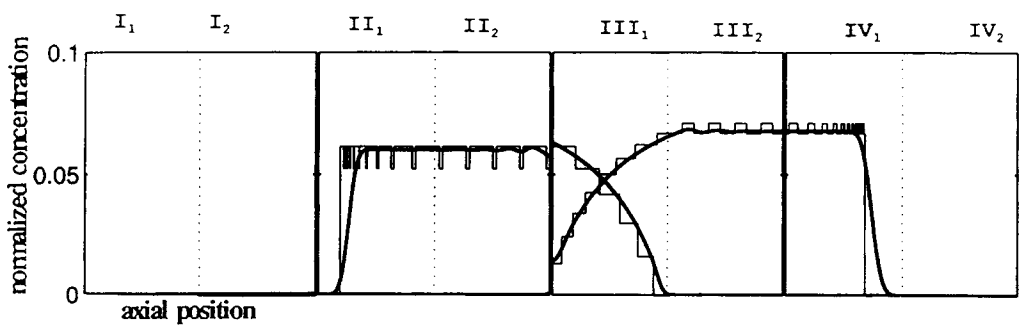

Figure 3b. Axial concentration profiles of the two-feed components at the end of a cycle under steady-state conditions.

Other experimental conditions as for Figure 3a. Thick solid lines, concentration profiles of raffinate and extract calculated with the nonideal model. Thin solid line, concentration profiles of raffinate and extract calculated with the ideal model.

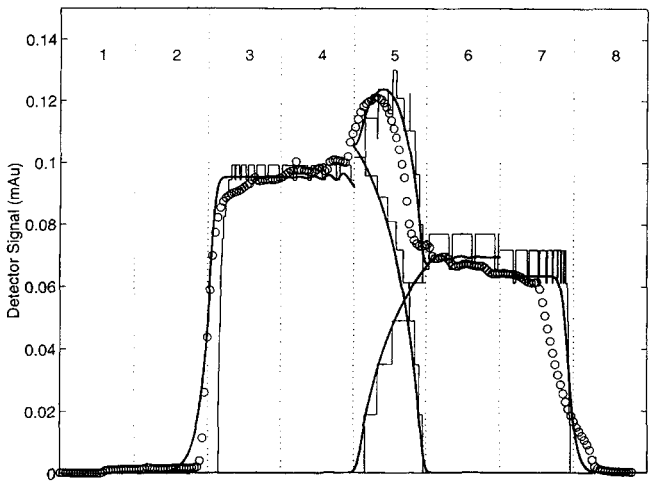

Figure 4a. Experimental results recorded with an on-line detector for $\beta_2 = \beta_3 = 1.15$ and $\beta_1 = \beta_4 = 1.03$.

Total porosity of the column, $\epsilon_T = 0.580$. Flow rates: $Q_I = 1.327$ mL/min; $Q_{II} = 1.035$ mL/min; $Q_{III} = 1.195$ mL/min; $Q_{IV} = 0.948$ mL/min. Switching time, $t^* = 9.38$ min. Feed composition, $C_1 = 0.150$ g/L; $C_2 = 0.132$ g/L. Otherwise, same parameters as for Figure 3a. Symbols, experimental data. Thick solid lines, concentration profiles of raffinate and extract calculated with the nonideal model. Thin solid line, concentration profiles of raffinate and extract calculated with the ideal model.

close to the end of column IV.1 (see Figure 4a). The low concentration part of the front of component 1 enters into this column when the column efficiency is finite. This result is illustrated in panel 2 of Figure 4a and in the box for column IV.2 in Figure 4b. This is explained by the location of the point at Λ_a^∞, which is very close to the boundary between the two columns. Only if dispersion were very small, would it bring no amount of component 1 into column IV.2. The low concentration part of the rear of the profile of component 2 in column I.1 penetrates into column I.2, as shown in panel 8 of Figure 4a and in the box for column I.2 of Figure 4b, for the same reason, finite mass transfer and axial dispersion. Thus, in this case, eight columns are necessary to achieve the separation with a satisfactory product purity. The analyses of the SMB effluents gave 99.8% of 3-phenyl propanol and 0.2% of 2-phenyl ethanol in the extract, 98.5% of 2-phenylethanol and 1.5% of 3-phenyl propanol in the raffinate.

In the third case (Figures 5a and 5b), $\beta_1 = \beta_4 = 1.03$ (as in the second case) and $\beta_2 = \beta_3 = 1.02$. In section II, $n_e = 5$, so it takes one fewer cycle than in the other two cases for the rear of component 2 to appear in column II.1. The values of L_0^d, L_d^4, and Λ_d^∞ are changed to $0.254L$, $0.250L$, and $1.693L$, respectively. $K_D = 0.338$, n_r is also reduced to 3, L_0^a, L_4^a, and Λ_a^∞ become equal to $0.338L$, $0.229L$, and $1.880L$, respectively. Again, eight columns are necessary to achieve the required separation. The mixing zone is much wider than in the previous two cases and involves panels 4, 5 and 6 (Figure 5a), compared to only panel 5 in Figures 3a and 4a. More feed input and a better average utilization of the stationary phase are achieved under these conditions. The analyses of the SMB effluents gave 97.9% of 3-phenyl propanol and 2.1% of 2-phenyl ethanol in the extract, 99.9% of 2-phenylethanol and 0.1% of 3-phenyl propanol in the raffinate.

Under no circumstance, should Λ_a^∞ and Λ_d^∞ be larger than $2L$. Because there is no possible compression effect between columns IV.1 and IV.2 nor between columns I.1 and I.2, if (within the framework of the ideal model) any concentration front enters either column IV.2 (a raffinate front coming from column IV.1) or column I.1 (an extract front coming from column I.2) it will be conveyed sooner or later to the end of this column and beyond, and will eventually contaminate the desorbent and the corresponding product. With actual columns, which have a finite efficiency, small concentrations of the two components do enter these columns, because of apparent axial dispersion. They result in an incomplete separation, but the product purity can be kept high by proper design and operation of the unit.

Furthermore, the experimental results showed that, when the values of β_j were changed, the number of cycles required to reach steady state also changed. Table 3 compares the values of the flow rates Q_F, Q_D, Q_R, and Q_E in the three different experiments. Note that, in the third case (see Figure 5a), a 96% increase of the feed rate and a 29% decrease of the desorbent flow rate (as compared to those set in the first case, see Table 3b) are achieved simultaneously, without changing the solid flow rate. The corresponding increase in the production rate and decrease in the solvent consumption of the unit are obtained by using more favorable conditions corresponding to Figure 5 rather than the moderate conditions corresponding to Figure 3. This demonstrates the interest and simplicity of an optimization procedure based on the use of the analytical solution of the ideal model.

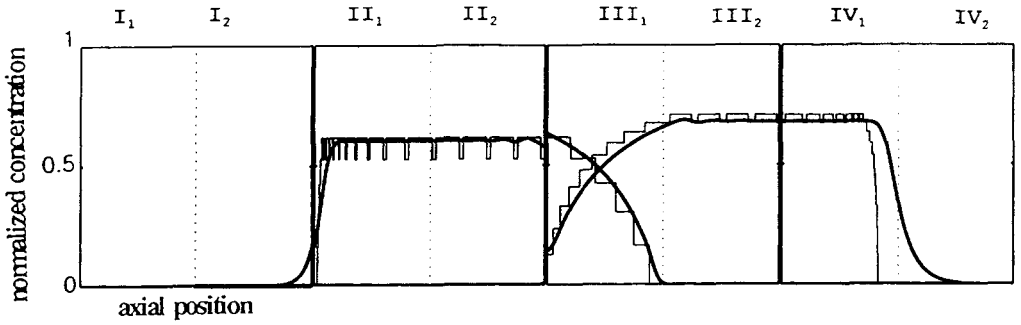

Figure 4b. Axial concentration profiles of the two-feed components calculated at the end of a cycle under steady-state conditions.

Same as Figure 3b but under the experimental conditions of Figure 4a.

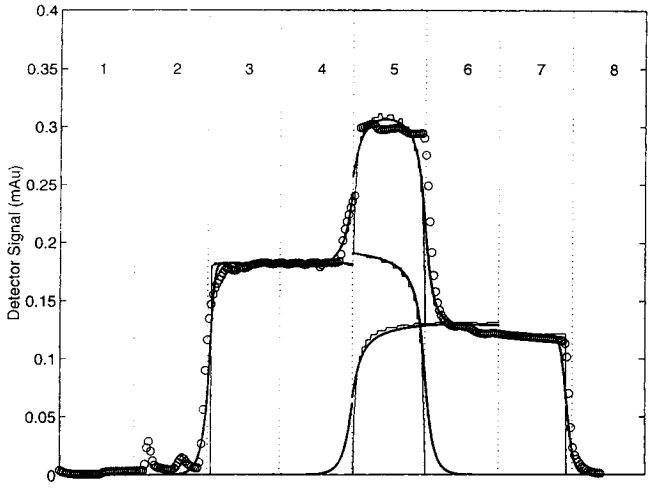

Figure 5a. Experimental results recorded with an on-line detector for $\beta_2 = \beta_3 = 1.02$ and $\beta_1 = \beta_4 = 1.03$.

Column total porosity, $\epsilon_T = 0.580$. Flow rates: $Q_I = 1.327$ mL/min; $Q_{II} = 0.971$ mL/min; $Q_{III} = 1.286$ mL/min; $Q_{IV} = 0.948$ mL/min. Switching time, $t^* = 9.38$ min. Feed composition: $C_1 = 0.130$ g/L; $C_2 = 0.127$ g/L. Symbols, experimental data. Thick solid lines, concentration profiles of raffinate and extract calculated with the nonideal model. Thin solid line, concentration profiles of raffinate and extract calculated with the ideal model.

Figures 6 and 7 illustrate the influence of β_2 and β_3 on the feed flow rate and the width of the mixed zone. Very large values (1.50) of either of these two parameters are used to calculate the band profiles. Since the feed flow rate has to be very low in these cases, one of the two products becomes much more concentrated than the other one. In Figure 6, the extract is more concentrated than the raffinate, the opposite being true in Figure 7. Although it might be useful to concentrate one product during the separation, this approach is not practical because of the low feed flow rate and the high dilution of the other component.

Conclusion

The important objective functions of the optimization of a chromatographic separation are the feed flow rate, which should be maximized to maximize the production rate, and the desorbent flow rate, which should be minimized to minimize the cost by reducing the dilution of the products and limiting the amount of solvent to regenerate and recycle. From Eq. B1a, it follows that the feed flow rate is maximum when both β_2 and β_3 are minimum, hence when $\beta_2 = \beta_3 = 1$. Similarly, the lowest possible desorbent flow rate is obtained when β_1 and β_4 are both as small as possible (Eq. B1d), i.e., when $\beta_1 = \beta_4 = 1$. However, it is not possible to operate an

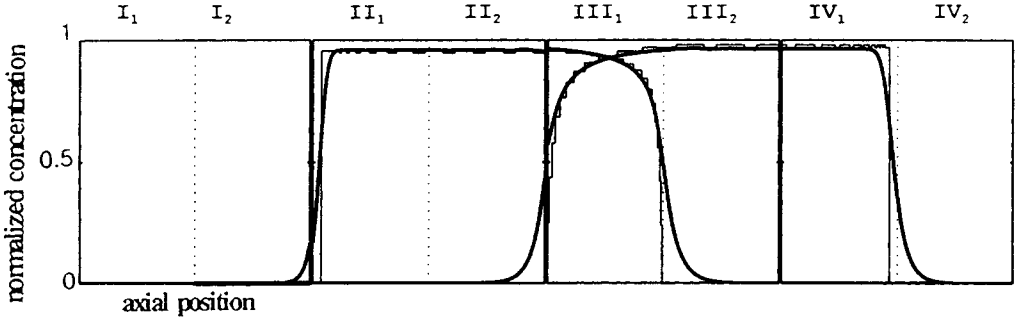

Figure 5b. Axial concentration profiles of two-feed components at the end of a cycle under steady-state conditions.

Same as in Figure 3b but under experimental conditions of Figure 5a.

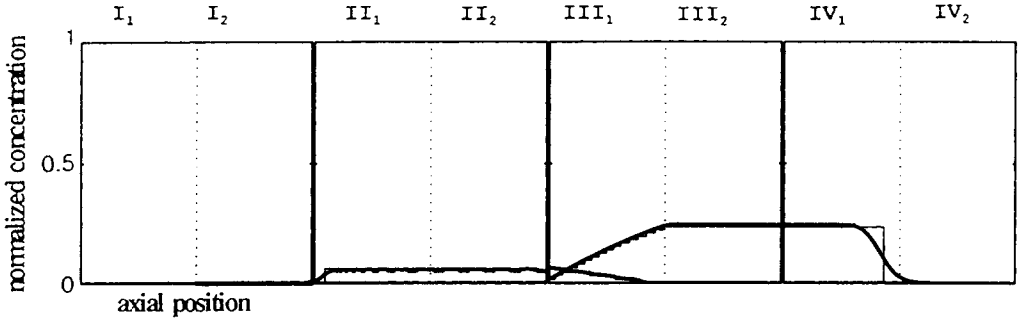

Figure 6. Axial concentration profiles of two-feed components at the end of a cycle under steady-state conditions.

Same as Figure 3b, except experimental conditions: $\beta_1 = 1.03$, $\beta_2 = 1.10$, $\beta_3 = 1.50$, and $\beta_4 = 1.03$. Column total porosity: $\epsilon_T = 0.572$. Flow rates: $Q_I = 1.336$ mL/min; $Q_{II} = 1.014$ mL/min; $Q_{III} = 1.031$ mL/min; $Q_{IV} = 0.950$ mL/min. Switching time: $t^* = 9.38$ min. Thick solid lines, concentration profiles of raffinate and extract calculated with the nonideal model. Thin solid line, concentration profiles of raffinate and extract calculated with the ideal model.

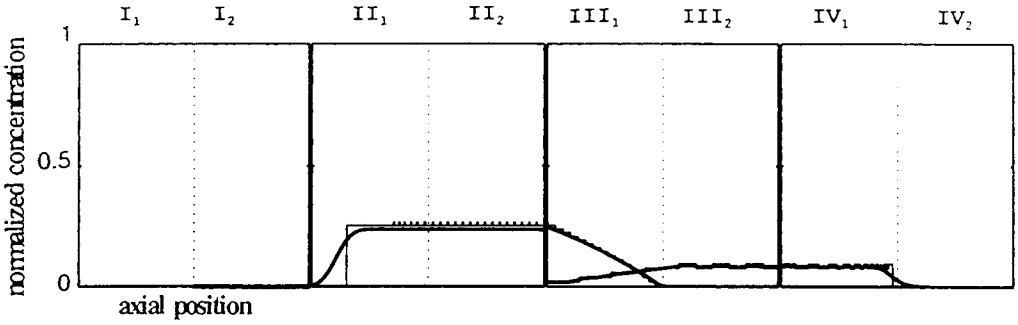

Figure 7. Axial concentration profiles of two-feed components at the end of a cycle under steady-state conditions.

Same as Figure 3b, except experimental conditions: $\beta_1 = 1.03$, $\beta_2 = 1.50$, $\beta_3 = 1.10$, and $\beta_4 = 1.03$. Column total porosity: $\epsilon_T = 0.572$. Flow rates: $Q_I = 1.336$ mL/min; $Q_{II} = 1.211$ mL/min; $Q_{III} = 1.234$ mL/min; $Q_{IV} = 0.944$ mL/min. Switching time: $t^* = 9.38$ min. Thick solid lines, concentration profiles of raffinate and extract calculated with the nonideal model. Thin solid line, concentration profiles of raffinate and extract calculated with the ideal model.

Table 3a. Values of the Input and Output Flow Rates Used in the Experiments*

	Q_F	Q_D	Q_R	Q_E
Figure 3	0.16 (100%)**	0.534 (100%)	0.299 (100%)	0.395 (100%)
Figure 4	0.16 (100%)	0.379 (71%)	0.247 (83%)	0.292 (74%)
Figure 5	0.315 (196%)	0.379 (71%)	0.338 (113%)	0.356 (90%)
Figure 6	0.017 (11%)	0.386 (72%)	0.081 (27%)	0.322 (82%)
Figure 7	0.023 (14%)	0.392 (73%)	0.290 (97%)	0.125 (32%)

Table 3b. Values of β_j Corresponding to the Flow Rates Used in the Experiments

	β_1	β_2	β_3	β_4
A	1.15	1.15	1.15	1.15
B	1.03	1.15	1.15	1.03
C	1.03	1.02	1.02	1.03
D†	1.03	1.50	1.10	1.03
E†	1.03	1.10	1.50	1.03

*All flow rates in mL/min.
**Proportion of corresponding flow rate for Figure 3.
†Calculations.

SMB with the unit value of any of the margin safety factor, let alone the four of them equal to 1. This would not be safe. Any fluctuation of one of the flow rates below its nominal value for any significant period of time would cause catastrophic failure of the unit. The smallest practical value of a coefficient β_j, $1+\epsilon$, results from the long-term pump stability and from the column-to-column fluctuations of the characteristics such as the permeability and the retention factors, which control the migration velocities of the bands. Considerable attention must be paid to the influence of the reproducibility of the column parameters in any study of optimization, stability and/or process control of SMB.

Our experimental results illustrate the algebraic solution of the ideal, linear model of SMB, which is the simplest and requires only a pocket calculator or a spreadsheet to implement. The concentration profiles obtained through these calculations are in excellent agreement with the experimental results, which validates the use of the solution. The axial dispersion observed with actual columns is easily accounted for by convolution with a Gaussian function. Thus, a simple tool is available to the engineer for the rapid optimization of the design of an SMB, allowing important savings over the approach conventionally used for the development of new separations.

Acknowledgments

This work has been supported in part by grant CHE-9201663 of the National Science Foundation and by the cooperative agreement between the University of Tennessee and the Oak Ridge National Laboratory. We acknowledge the support of Maureen S. Smith in solving our computational problems.

Notation

A = column section, cm^2
K = isotherm derivative, in linear case, $K_i = a_i$
$K_A, \ldots, K_E$ = parameters in the algebraic solution of the ideal, linear model of SMB
L = column length or migration distance of a front, cm
$L_0^a, \ldots, L_0^d$ = parameters in the algebraic solution of the ideal, linear model of SMB
n = cycle rank
p = cycle number
q = solid-phase concentration, g/L

Q = flow rate, mL/s
t = time, s
t^* = cycle time, s
u = liquid-phase flow velocity, cm/s
z = axial position, cm
α = separation factor
β = ratio of the mass-flow rates in solid and liquid phases, in column j ($\beta_j > 1$)
γ = margin parameters in TMB
ϵ_T = column total porosity
Λ = migration distance of a front, cm

Superscripts

a = component 1 in column IV
b = component 2 in column III
c = component 1 in column III
d = component 2 in column II
in = column inlet
out = column outlet

Subscripts

D = desorbent
E = extract
F = feed
n = cycle rank
R = raffinate
S = solid
i = feed component ($i = 1, 2$)
j = section (j = I, ..., IV)

Literature Cited

Adachi, S., "Simulated Moving Bed Chromatography for Continuous Separation of Two Components and Its Application to Bioreactors," *J. Chromatog. A*, **658**, 271 (1994).

Barker, P. E., K. England, and G. Vlachogiannis, "Mathematical Model for the Fractionation of Dextran on a Semi-continuous Counter-Current Simulated Moving Bed Chromatograph," *Chem. Eng. Res. Des.*, **61**, 241 (1983).

Broughton, D. B., "Production-Scale Adsorptive Separations of Liquid Mixtures by Moving-Bed Technology," *Sep. Sci. Technol.*, **19**, 723 (1985).

Charton, F., and R. M. Nicoud, "Complete Design of a Simulated Moving-Bed," *J. Chromatog. A*, **702**, 97 (1995).

Ching, C. B., and D. M. Ruthven, "An Experimental Study of a Simulated Countercurrent Adsorption System: I. Isothermal Steady State Operation," *Chem. Eng. Sci.*, **41**, 877 (1985).

Fish, B. B., R. W. Carr, and R. Aris, "Design and Performance of a Simulated Counter-Current Moving-Bed Separator," *AIChE J.*, **39**, 1783 (1995).

Ganetsos, G., and P. E. Barker, *Preparative and Production Scale Chromatography*, M. Dekker, New York (1993).

Guiochon, G., S. G. Shirazi, and A. M. Katti, *Fundamentals of Preparative and Nonlinear Chromatography*, Academic Press, Boston (1994).

Howard, A. J., G. Carta, and C. H. Byers, "Separation of Sugars by Continuous Annular Chromatography," *Ind. Eng. Chem. Res.*, **27**, 1873 (1988).

Lim, B. G., C. B. Ching, R. B. H. Tan, and S. C. Ng, "Recovery of (−)-Praziquantel from Racemic Mixtures by Continuous Chromatography and Crystallisation," *Chem. Eng. Sci.*, **50**, 2289 (1995).

Ruthven, D. M., and C. B. Ching, "Countercurrent and Simulated Countercurrent Adsorption Separation Processes," *Chem. Eng. Sci.*, **44**, 1011 (1989).

Stinson, S. C., "Chiral Drugs," *Chem. and Eng. News*, 44 (Oct. 9, 1995).

Storti, G., M. Mazzotti, M. Morbidelli, and S. Carra, "Robust Design of Binary Countercurrent Adsorption Separation Processes," *AIChE J.*, **39**, 471 (1993).

Yun, T., "A Fundamental Study of Simulated Moving Bed Chromatography," PhD Diss., Univ. of Tennessee, Knoxville (1996).

Yun, T., G. Zhong, and G. Guiochon, "Simulated Moving Bed under Linear Conditions: Experimental vs. Calculated Results," *AIChE J.*, **43**, 935 (1997).

Zhong, G., and G. Guiochon, "Analytical Solution for the Linear Ideal Model of Simulated Moving Bed Chromatography," *Chem. Eng. Sci.*, **51**, 4307 (1996).

Zhong, G., M. S. Smith, and G. Guiochon, "Effect of the Flow Rates in Linear, Ideal, Simulated Moving Bed Chromatography," *AIChE J.*, **43**, 2960 (1997).

Zhong, G., T. Yun, P. Sajonz, and G. Guiochon, "Simulated Moving Bed Chromatography: Effect of Section Subdivision in Linear Ideal Case," in preparation (1997).

Appendix A: Algebraic Solution of the Ideal, Linear SMB Model

It describes briefly the algebraic solution of the ideal, linear model of SMB with two columns per section and different values of β_j in each of its four sections with two columns. The detailed derivation of the solution in the simple case of an SMB with four columns and identical values of β in each section was given by Zhong and Guiochon (1996). The extension of this solution to any number of columns in each one of the four sections, but $\beta_j = \beta$, $\forall i$, was discussed by Zhong et al. (1997). A review of the general solution and its applications is in preparation. The solution described here is at the end of a cycle, which is why section I will be empty for an effective SMB.

Typical solutions for an intermediate number of cycles and for an infinite number, corresponding the steady-state solution, are shown in Figures A1a and A1b, respectively. The profiles of the two feed components along the SMB are staircases, which are defined by the step height and by the position of its front. A new step is formed in each profile, at the beginning of each new cycle, originating at the feed inlet, between sections II and III (Figure A1). This step migrates at a constant velocity along the corresponding section (linear isotherm) and eventually penetrates into either section I (extract) or IV (raffinate). In these sections, the migration rate of the step front is lower than that in the corresponding central sections and the front of either band tends toward a stable limit.

The concentration of the successive steps observed in the concentration profiles at the end of the nth cycle is given by

$$C_{\mathrm{I}}^{pt^*} = (1 - K_A^p) C_{i,F} \tag{A1}$$

where p is an integer smaller than or equal to the cycle rank, n. The highest concentration is obtained for $p = n$, at least in the first few cycles. However, only a finite number of steps is observed in the profiles because each step has a finite length in the central sections, so that a column can hold a finite number of them. For simplification, the following parameters (including K_A in Eq. A1) are defined:

$$K_A = \frac{1 + FK_1\beta_2}{1 + FK_2/\beta_3} \tag{A2a}$$

$$K_B = \frac{1 + FK_1/\beta_4}{1 + FK_2/\beta_3} \tag{A2b}$$

$$K_C = \frac{1 + FK_1\beta_2}{1 + FK_2\beta_1} \tag{A2c}$$

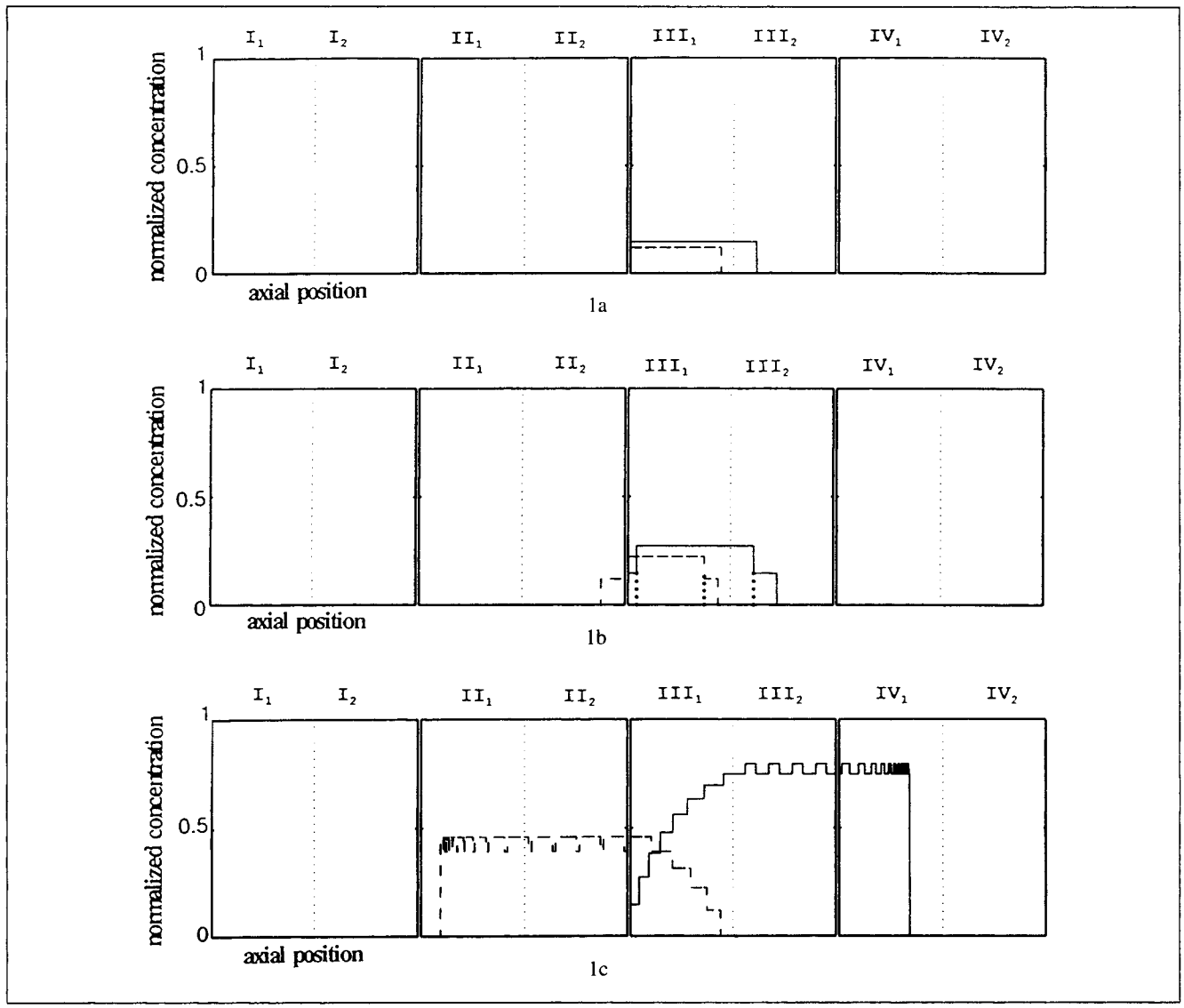

Figure A1. Axial concentration profiles of the two-feed components.

1a. At the end of the first cycle; 1b. at the end of the second cycle; 1c. under steady-state (asymptotic) conditions.

$$K_D = \frac{F(K_2/\beta_3 - K_1)}{1 + FK_1} \tag{A2d}$$

$$K_E = \frac{1 + FK_1/\beta_4}{1 + FK_1} \tag{A2e}$$

The other two parameters just defined, K_B and K_C, will be used in the next sections.

During each cycle, the front and rear concentration steps of the profiles of the two components move by distances which are expressed simply as a function of the following characteristic distances:

$$L_0^a = \frac{F(K_2/\beta_3 - K_1)}{1 + FK_1} L \tag{A3a}$$

$$L_0^b = \frac{FK_2(1 - 1/\beta_3)}{1 + FK_2} L \tag{A3b}$$

$$L_0^c = \frac{FK_1(\beta_2 - 1)(1 + FK_2/\beta_3)}{(1 + FK_1)(1 + FK_1\beta_2)} L \tag{A3c}$$

$$L_0^d = \frac{F(K_2 - K_1\beta_2)}{1 + FK_2} L \tag{A3d}$$

The locations of different steps are derived following the same approach as described by Zhong and Guiochon (1996), but we must distinguish two cases, depending on whether the band front in a section is still in the column nearest to the feed port or has already entered into the second column. The equations giving the step positions are different in these two cases.

Concentration profiles in section II

At the beginning of the second cycle, the extract enters column II.2. Then, during each new period, the front of the first step (height, C_2^{r*}, Eq. A1) moves backward along this column by a constant distance, because this step is either in column II.1 or in column II.2 depending on the time spent since the beginning of the current cycle. In both cases, the liquid flow velocity is the same. For $n < n_e$, the profile of the extract is the same whether there are one or two columns in section II. For a certain cycle rank, n_e, the profile front enters into column II.1. For $n > n_e$, the profiles in the two columns differ (Zhong et al., 1997).

Beginning of Startup: $n \le n_e$. In this case, at the end of each successive cycle, the extract is found in the second column of the second section (column II.2). During each cycle, the front of the first step moves backward by the same distance L_0^d given by Eq. A3d. It will eventually remain in column II.1 at the end of the cycle of rank n_e, such that

$$n_e - 2 \le L/L_0^d < n_e - 1 \tag{A4}$$

For any cycle of rank n ($3 \le n < n_e$), the width of each step at the rear of the extract profile equals L_0^d.

Cycle of Rank $(n_e + 1)$. For the second time, the rear of the extract profile ends its backward migration inside the first column of the section, column II.1. From now on, the rear of this profile will migrate longer and longer in column I during the first part of the cycle (the flow rate is higher in section I than that in section II, and the front is farther backward in column I.2 at the beginning of each cycle). The step width begins to decrease and tends toward 0. In this case, the width of the lowest step of the extract concentration plateau increases by $L_{n_e-1}^d$, given by

$$L_{n_e-1}^d = L_0^d - (1 - K_C)\delta^d \tag{A5}$$

with L_0^d given by Eq. A3d and $\delta^d = (n_e - 1)L_0^d - L$.

Further Cycles, with $n > (n_e + 1)$. For any cycle of rank n larger than $n_e + 1$, the backward migration distance of the first step of the rear part of the extract profile increases by the distance:

$$L_n^d = K_C^{n-n_e-1} L_{n_e-1}^d \tag{A6}$$

The length of each successive backward migration distance decreases by the factor K_C (< 1). The width of any successive step of the staircase at the rear of the extract profile in column II.1 is wider than that of the lower one. This phenomenon is obviously due to the fact that, during the first part of the cycle, the rear of the extract band (which has moved from column II.1 to column I.2 at the beginning of the cycle) drifts along section I at a velocity higher than during the second part of the cycle, when it is in section II, where the velocity is lower. K_C results from the combination of these two velocities. This phenomenon was explained in more detail by Zhong and Guiochon (1996).

Steady State. The steady state is reached in an asymptotic sense. The position of the rear of the extract band is obtained by summing up the widths of all the steps. This asymptotic position is given by

$$\Lambda_\infty^d = \sum_{p=1}^{n_e-2} L_p^d + \frac{L_{n_e-1}^d}{1 - K_C} < 2L \tag{A7}$$

This condition is necessary for proper operation of an SMB as a separator. Otherwise, the extract would move into the raffinate stream.

Note that the asymptotic property exists only in the first column of section II (II.1), not in the second one. In column II.2, a rectangular concentration wave takes place. This situation differs from the one in the conventional four-column configuration of SMB. The difference is explained by the presence of the extra column II.2 between columns II.1 and section III. Compression of these waves takes place between columns II.1 and I.2.

Concentration profiles in section III

The consequences for the algebraic solution of having two columns instead of one in section III are quite similar to those observed in the case of section II. The front of the raffinate band profile ends in a staircase which, at the beginning of the startup, penetrates in column III.2, deeper and deeper, and eventually enters into section IV (column IV.1). It ends in the other staircase which begins at the feed inlet, in column III.1. Each step has a concentration given by Eq. A1. To obtain the step positions, we first define a cycle rank, n_r, such that the front of the raffinate profile remains in column III.2 at cycle end when the number of cycles is lower than n_r and that this front ends up in section IV after n_r cycles or more. Note that the raffinate is produced only when $n > n_r$. The discussion is similar to the one in the previous section. Finally, when the separation factor is very large, the front of the raffinate may enter into column IV.1 during the first cycle. This rare case is not discussed here.

Beginning of the Startup: $n < n_r$. The raffinate front ends first in section III (column III.2). n_r is given by the following relationship

$$n_r - 1 \le \frac{L}{L_0^a} = \frac{1}{K_D} < n_r \tag{A8}$$

For any cycle of rank n such that $n \le n_r$, the front of the last descending step of the raffinate front migrates downstream by the same distance

$$L_{n-1}^a = L_0^a \tag{A9}$$

In Eqs. A8 and A9, L_0^a is given by Eq. A3a. During each successive cycle ($n < n_r$), the front of the raffinate migrates by the same distance, L_0^a.

$b - n = n_r$. The raffinate front moves from column III.2 into column IV.1 for the first time during cycle n_r. The migration distance of the first step is

$$L^a_{(n_r)} = \{K_E - K_B + (1 - K_B)[1 - (n_r - 1)K_D]\}L \quad \text{(A10)}$$

$c - n = n_r + 1$.

At the end of the second cycle during which the raffinate front moves into section IV, the migration distance of the first step of the front of the raffinate profile is

$$L^a_{n_r+1} = K_B[K_D + (1 - nK_D)(1 - K_B)]L \quad \text{(A11)}$$

The parameters K_A, K_B, K_C, K_D and K_E are given in Eqs. A2a–e.

$d - n > n_r + 1$.

The raffinate front has now been in section IV more than twice at the end of a cycle. If the raffinate front ends up in section IV for p cycles, with $2 \le p$, the migration distance of the raffinate front is

$$L^a_{n_r+p} = K_B^{p-2} L^a_{n_r+1} \quad \text{(A12)}$$

Steady State. Steady-state condition is reached asymptotically. Summing up the widths of all the successive migration distances of the concentration step at the front of the raffinate profile gives the asymptotic position of the concentration front in section IV.

$$\Lambda^a_\infty = \sum_{n=1}^{n_r} L^a_n + \frac{L^a_{n_r+1}}{1 - K_B} < 2L \quad \text{(A13)}$$

The condition is required for the front of the raffinate band to end up in section IV at the end of a cycle. In the rare case in which the raffinate front enters section IV during the very first cycle, a different equation applies (Zhong et al., 1997).

The asymptotic convergence of the raffinate front takes place in section IV. In column III.2, the concentration profile is a succession of square oscillations of constant period. No compression of this part of the profile does take place. Compression can take place only between columns III.2 and IV.1 because the liquid flow velocity is different in sections III and IV. The advantage of using several columns in section III is that it gives the possibility to achieve a higher purity of the raffinate by limiting the consequences of the apparent axial dispersion which takes place in practice.

Feed Sides of the Steady State Profiles. The feed sides of the two component profiles are found in section III. Length increments L^b_0 and L^c_0, similar to L^a_0 and L^d_0, can be defined (Figures A1 to A3). They are given by Eqs. A2b and A2c. For the following steps, we obtain

$$L^b_{n-1} = \frac{1}{K_A^{n-1}} L^b_0 \quad \text{(A14a)}$$

$$L^c_{n-1} = \frac{1}{K_A^{n-1}} L^c_0 \quad \text{(A14b)}$$

The sum of these migration distances does not tend toward a limit when n increases indefinitely, which is why there is a finite number of steps in these profiles (Zhong and Guiochon, 1996).

Concentrations profiles in sections I and IV

Placing more than one column in either section I or IV does not seem to have an impact, since the raffainte remains in the first column of section IV and the extract in the last column of section II once stability conditions are met. However, in the case of an actual SMB, using real columns of finite efficiency, the use of a second column considerably reduces the effect of axial dispersion on the pollution of the extract by the raffinate (see Figures 3a, 4a, and 5a).

Appendix B: Constraints on β_j Values

The system of the linear Eqs. 7a–7d can easily be solved by eliminating Q_1 between them:

$$Q_F = Q_S(K_2/\beta_3 - K_1\beta_2) \quad \text{(B1a)}$$

$$Q_E = Q_S(K_2\beta_1 - K_1\beta_2) \quad \text{(B1b)}$$

$$Q_R = Q_S(K_2/\beta_3 - K_1/\beta_4) \quad \text{(B1c)}$$

$$Q_D = Q_S(K_2\beta_1 - K_1/\beta_4) \quad \text{(B1d)}$$

The fourth equation stems from the integral balance $Q_D + Q_F = Q_E + Q_R$ which states steady-state conditions in the SMB unit.

To make physical sense, all the flow rates must be positive. The fact that the four terms between parentheses in the righthand side of Eqs. B1 are positive (with $\alpha = K_2/K_1$) gives the following set of conditions:

$$\beta_3\beta_2 < \alpha \quad \text{(B2a)}$$

$$\beta_2/\beta_1 < \alpha \quad \text{(B2b)}$$

$$\beta_3/\beta_4 < \alpha \quad \text{(B2c)}$$

$$\frac{1}{\beta_1\beta_4} < \alpha \quad \text{(B2d)}$$

By systematically combining the definition of β_j, Eqs. 5 and 7, and applying the condition in the corresponding Eqs. 6, we

obtain the following second set of conditions which must be satisfied.

$$\beta_1 > \frac{1}{\alpha}, \quad \beta_1 > 1 \tag{B3a}$$

$$\beta_2 > 1, \quad \beta_2 < \alpha \tag{B3b}$$

$$\beta_3 < \alpha, \quad \beta_3 > 1 \tag{B3c}$$

$$\beta_4 > 1, \quad \beta_4 > 1/\alpha \tag{B3d}$$

From the system of Eqs. B3, it follows that both β_2 and β_3 must be between 1 and α and that both β_1 and β_4 must be larger than 1 (α is larger than 1 by definition), which makes Eq. B2d always satisfied. Then, the two sets of conditions can be simplified and combined into

$$\beta_j > 1, \quad \forall i \tag{B4a}$$

$$\beta_2/\beta_1 < \alpha \tag{B4b}$$

$$\beta_2 \beta_3 < \alpha \tag{B4c}$$

$$\beta_3/\beta_4 < \alpha \tag{B4d}$$

Since both β_2 and β_3 must be smaller than α, Eqs. B4b and B4d are always verified because of Eq. B4a. Thus, they can be dropped without loss of rigor and the set of conditions is reduced to

$$\beta_j > 1, \quad \forall i \tag{B5a}$$

$$\beta_2 \beta_3 < \alpha \tag{B5b}$$

This is the set of conditions illustrated in Figures 2a and 2b.

Manuscript received Mar. 21, 1997, and revision received July 29, 1997.